Journal of Petroleum Exploration and Production Technology
https://doi.org/10.1007/s13202-024-01796-6

ORIGINAL PAPER-PRODUCTION GEOLOGY

Pore throat distributions and movable fluid occurrences in different diagenetic facies of tight sandstone reservoirs in the Triassic Chang 6 reservoirs, Wuqi Area, Ordos Basin, China

Pan Li[1,2] · Yangcheng Ou[3] · Hualin Chen[3] · Qiang Li[4] · Lei Zhao[3] · Jian Yan[1,2]

Received: 21 November 2023 / Accepted: 19 March 2024

Abstract

The 6th member of the Triassic Yanchang Formation, hereafter referred to as Chang 6 reservoir, in the Wuqi area of the Ordos Basin presents formidable obstacles for efficient tight oil development. This reservoir is known for its tight lithology, strong heterogeneity, inadequate oil saturation, and abnormally low reservoir pressure, which collectively contribute to the highly differentiated mobility of tight oil within the formation. To overcome these challenges, a comprehensive understanding of the factors influencing oil mobility is essential. This study investigates the occurrence characteristics of movable fluids in different diagenetic facies and the corresponding influential factors by employing various microscopic experiments, including high-pressure mercury intrusion, constant-rate mercury intrusion, nuclear magnetic resonance test, scanning electron microscopy, pore-casted thin section analysis, and X-ray diffraction measurement. There is a weaker correlation between the pore-throat radius ratio and the movable fluid saturation in reservoirs of various diagenetic facies ($R^2 = 0.6104$), whereas there is a stronger correlation between movable fluid saturation and throat radius ($R^2 = 0.9415$). Among the seven types of diagenetic facies, chlorite membrane cementation-intergranular pore facies (Facies I) and chlorite and illite membrane cementation-intergranular pore facies (Facies II) have the best-developed throats and the highest coordination number. Illite cementation-intergranular pore facies (Facies III) and illite and chlorite membrane cementation-dissolution facies (Facies IV) demonstrate smaller pore-throat radii and moderate to poor reservoir connectivity. The other three facies, namely illite cementation-dissolution facies (Facies V), illite cementation facies (Facies VI), and carbonate tight cementation facies (Facies VII) exhibit underdeveloped pore structures and lower recovery rates. Pore-throat radius emerges as the principal factor influencing reservoir permeability and storage capacity. The distribution of favorable diagenetic facies is influenced by depositional environments, diagenetic processes, and microscopic pore-throat characteristics. This study significantly enhances our understanding of the differential occurrence characteristics of fluids in different diagenetic facies in the Chang 6 reservoir, providing valuable insights for future exploration and production endeavors aimed at optimizing oil recovery in tight sandstone reservoirs.

Keywords Various diagenetic facies · Tight sandstone reservoir · Movable fluid occurrences · Pore and throat distributions · Ordos Basin

✉ Pan Li
dr.lipan@qq.com

[1] College of Petroleum Engineering, Xi'an Shiyou University, Xi'an 710065, China

[2] Cooperative Innovation Center of Unconventional Oil and Gas Exploration and Development, Xi'an Shiyou University, Xi'an 710065, Shaanxi, China

[3] Geological Exploration and Development Research Institute, CNPC Chuanqing Drilling Engineering Company Limited, Chengdu 610051, China

[4] PetroChina Changqing Oilfield Company, No.8 Oil Production Plant, Xi'an 710018, China

Introduction

Diagenetic facies significantly influence reservoir performances, making them a focal point in current hydrocarbon exploitation studies (Lai et al. 2016). They are particularly significant during the formation of the tight sandstone reservoirs, as diagenetic processes in clastic rocks profoundly impact their development. The occurrence and characteristics of diagenetic processes are influenced by complex and variable environmental conditions, which, in turn, determine the internal and external factors affecting reservoir tightness

Published online: 23 April 2024

(Wang et al. 2020a, b). The space within reservoir rocks constitutes a complex, three-dimensional network. Within this intricate network, all spaces can be categorized based on their functions in the storage and movement of fluids, specifically into two types: pores and throats. Pores are the spaces in the rock framework that are not occupied by solid matter, usually filled with gasses, liquids, or solids. They are characterized as relatively larger spaces enclosed by the framework grains, playing a substantial role in fluid storage. On the other hand, throats are the comparatively narrower segments that may not significantly contribute to increasing the pore volume, yet are essential in linking the pores, thereby forming effective channels for fluid transport (Wang and Zeng 2020; Huang et al. 2021). Diagenetic facies offer a comprehensive representation of particles, cementation, fabric, and pore evolution. As such, they serve as valuable indicators of reservoirs that have undergone different types and stages of diagenetic modifications. Utilizing diagenetic facies has emerged as a novel and widely applied method for predicting high-quality reservoirs across various fields of oil and gas exploration. Previous studies have employed diverse approaches to classify reservoir types, with diagenetic facies being a primary classification scheme based on essential physical properties, including lithology, petrophysical characteristics, and so on (Al-Mahrooqi et al. 2006; Liu et al. 2020b).

As oilfield development progresses, the intricate diagenetic processes and diverse diagenetic types pose constraints on understanding the reservoir properties. The presence of nano-scale to micro-scale pores as well as the strong heterogeneity of reservoirs hinder detailed descriptions and quantitative characterizations, thereby impacting efficient oilfield development. Diagenetic facies directly reflect features of present-day reservoirs and serve as genetic indicators of the variations in micro-pore structures within them. Further research on diagenetic facies can help elucidate the occurrence characteristics of movable fluids across various micro-pore structures. Despite the progress in studying diagenetic facies, there is currently a lack of a unified standard for the naming and classification of diagenetic facies. Generally, naming conventions rely on combinations of diagenetic processes, cementation, and pore types, with limited considerations of diagenetic intensities (Yang et al. 2013; Xu et al. 2020; Zhang et al. 2020). Moreover, diagenetic facies represent a classification scheme for reservoir types based on fundamental physical properties, such as lithology and petrophysical characteristics. They provide a comprehensive summary of the influences of depositional and diagenetic processes on reservoirs. Particularly for low-permeability reservoirs that have undergone complex diagenetic processes, the subdivision of diagenetic facies holds significant practical importance for predicting reservoir distribution, identifying favorable areas, and evaluating reservoir quality. Therefore, it becomes essential to conduct meticulous analyzes of flow features in microscopic pore throats in various diagenetic facies types at the microscopic level (Daigle and Johnson 2016; Qiao et al. 2020a, b). Such investigations will enhance our understanding of the reservoir's properties and facilitate more effective decision-making in oilfield development strategies.

Prior studies have predominantly focused on quantifying movable fluid parameters, with less emphasis on the examination of movable fluid occurrence characteristics and the factors influencing them. Movable fluid saturation, a critical saturation value obtained through nuclear magnetic resonance (NMR) experiments, offers insights into fluid occurrence within pore structures. By assessing movable fluid saturation, the reservoir's pore structure can be rapidly and intuitively evaluated. This evaluation is particularly beneficial for effectively gauging developmental impacts in low permeability sandstone reservoirs. Furthermore, NMR-based assessments of movable fluid saturation provide crucial data, enabling detailed characterization of microscopic pore structures and analysis of the variable characteristics and disparities of movable fluids within the reservoir.

Movable fluid saturation is a pivotal parameter in assessing reservoir performance as well as calculating reserves of hydrocarbons. It holds significant value in reflecting micropore structure and fluid distribution within the pores (Yao and Liu 2012; Chen et al. 2017a; Xu et al. 2021). NMR has been widely used for analyzing the fluid flow features, including permeability of pores as well as saturations of movable fluids (Li et al. 2017; Testamanti and Rezaee 2017; Mao et al. 2020). A comprehensive understanding has been achieved in previous studies about various diagenetic types, pore evolution processes, and diagenetic facies, by integrating several experiments (Dai et al. 2019; Liu et al. 2020a; Nie et al. 2021). Furthermore, the impact of different diagenetic facies types on movable fluid occurrences has been explored, specifically focusing on the Chang 6 reservoir. Lastly, the favorable reservoir types for efficient reservoir development have been identified. Results of this study are expected to provide important reference for effectively developing similar reservoirs in other oilfields (Chen et al. 2017b; Liu et al. 2018a, b; Wang et al. 2018; Yan et al. 2020; L. Wang et al. 2023a; L. Wang et al. 2023b).

To enhance the accuracy of reservoir quality characterization using fluid saturation parameters and to investigate the occurrence characteristics of movable fluids across various diagenetic facies, this study employed comprehensive NMR measurements. These measurements facilitate a quantitative analysis of the occurrence characteristics of movable fluids in the Chang 6 reservoir. Additionlly, a series of microscopic experiments were conducted to investigate the primary factors governing the diverse occurrence characteristics of these fluids. Our research identified seven types of diagenetic

facies within the study area, each exhibiting significant differences in microscopic pore structure. These variations in pore structure were found to have a direct influence on the distribution and presence of movable fluids in the reservoir.

Experimental section

Geological background

The Ordos Basin includes six tectonic units: the Yimeng uplift in the north, the Weibei uplift in the south, the western margin thrust belt and the Tianhuan depression in the west, the Jinxi flexure belt in the east, and the Yishan slope in the center. The basin is characterized by the development of multiple sets of source-reservoir-cap rock combinations, with abundant oil and gas resources. The Chang 6 reservoir is the most important oil-bearing reservoir, accounting for nearly 50% of the proven reserves in the Yanchang Formation. The study area, herein the Wuqi area, features a monocline with eastern strata higher than the western strata (Cui et al. 2019; Liu et al. 2018a, b; Huang et al. 2018). It is known for abundant hydrocarbon resources, with oil-bearing Chang 6 reservoir as the target layer for this study. Previous research has identified several challenges associated with the Chang 6 reservoir development, including high heterogeneity, complex and diverse micro-pore structures, and limited fluid mobility (Zang et al. 2022; Jiang et al. 2023a, b). Previous research has explored diagenetic stages of various reservoirs through the establishing pore evolution models, exploring impacts of diagenetic processes on petrophysical properties. However, there has been limited research about movable fluid occurrences and corresponding mechanisms across various types of diagenetic facies. To address this knowledge gap, this study employed NMR technology to quantitatively characterize movable fluid occurrences across various types of diagenetic facies, accompanied by comprehensive microscopic experiments (Fig. 1).

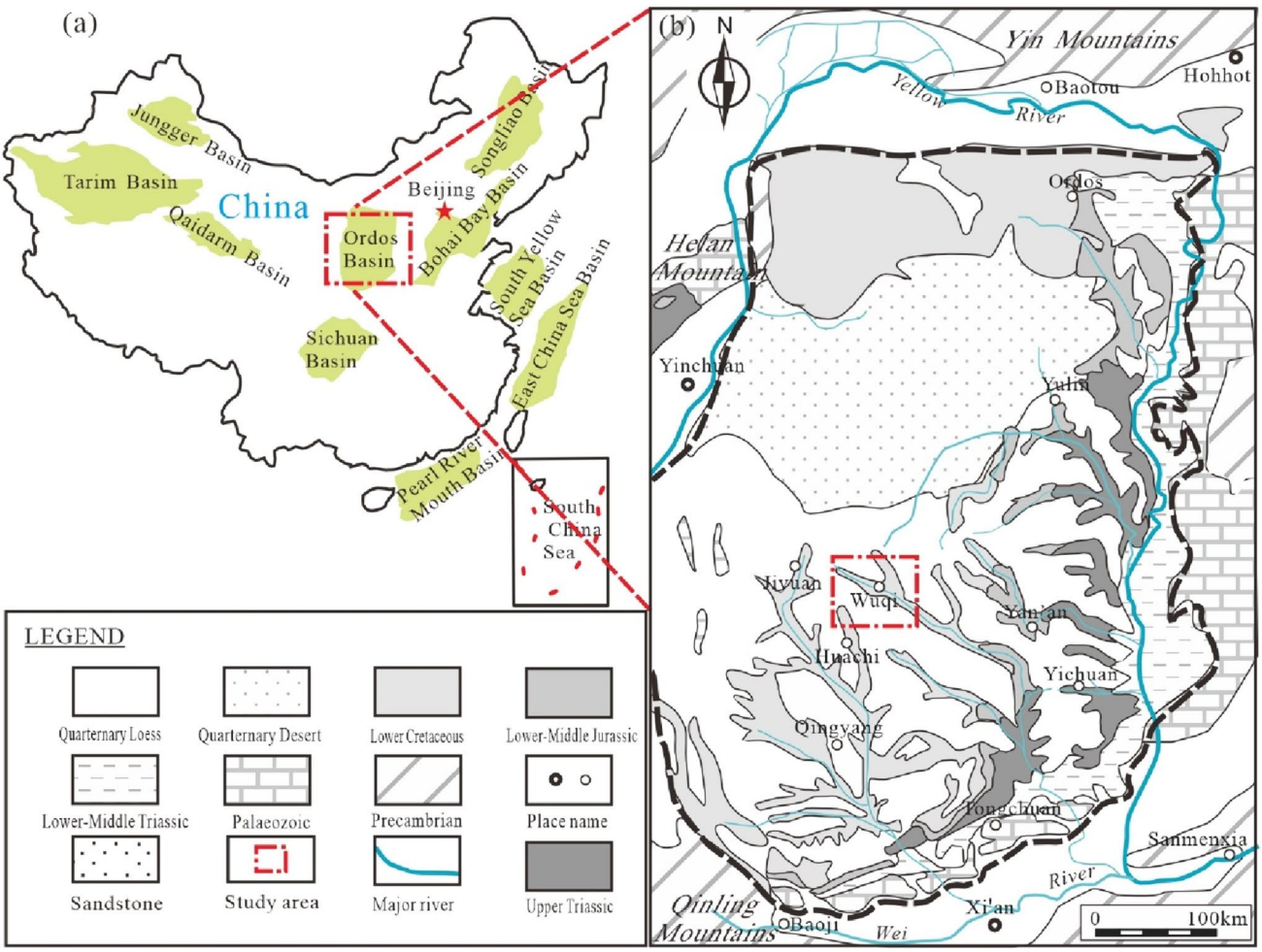

Fig. 1 Geographical locations of the study area

Table 1 NMR-based parameters about movable fluid saturation across various types of diagenetic facies

Facies type	Diagenetic facies	Water-filled porosity (%)	Air-filled porosity (%)	Gas permeability ($\times 10^{-3}\mu m^2$)	Movable fluid saturation (%)	Movable fluid porosity (%)	Bound water saturation (%)
Facies I	Chlorite membrane cementation-intergranular pore facies	10.02	7.09	0.19	49.5	4.96	50.5
Facies II	Chlorite and illite membrane cementation-intergranular pore facies	9.77	6.67	0.09	35.93	3.51	64.07
Facies III	Illite cementation-intergranular pore facies	8.63	6.92	0.12	34.18	2.95	65.82
Facies IV	Illite and chlorite cementation and dissolution facies	7.76	6.34	0.07	34.02	2.64	65.98
Facies V	Illite cementation and dissolution facies	10.36	5.37	0.12	20.37	2.11	79.63
Facies VI	Illite cementation facies	7.59	4.98	0.08	14.62	1.11	85.38
Facies VII	Carbonate tight cementation facies	5.67	2.67	0.03	11.46	0.65	88.54

Experiments and samples

NMR experiment

(1) Experimental principle

After rock samples were vacuumed and saturated with fluids, the T_2 relaxation time spectrum of fluids within pores was influenced by interaction forces between the fluid molecules and the pore surfaces. This spectrum revealed a notable distinction between bound fluids and movable fluids within pore space. As the centrifugal force was gradually increased, fluids were progressively displaced from pores, reducing NMR signals. Upon reaching a certain centrifugal force level, the NMR signal stabilized, indicating that further fluid removal became negligible. By analyzing the NMR signal under this critical centrifugal force, in conjunction with the signal from the fluid-saturated water, it was feasible to establish the cut-off value of T_2 (i.e., the boundary between the left and right peaks) and calculate the critical pore throat radius value. This calculation allowed for determining pore throat radius. As a result, the fluid occurrence state could be assessed using the T_2 spectrum, and a quantitative value for the movable fluid saturation could be obtained (Li et al. 2018).

(2) Rock samples and fluids

Table 1 shows the basic parameters of analyzed rock samples. Standard saline water (salinity of 5000 mg/L) was used to simulate the formation water.

(3) Experimental steps

The samples were first washed and then dried, followed by nitrogen-based measurements of permeability and porosity and saturation with formation water in the vacuum state and under pressure, yielding the water-filled porosity. Then, the T_2 spectrum was measured to further examine the properties of the saturated formation water. Subsequently, centrifuge experiments were conducted on the rock samples, with applied varying centrifugal forces of 21, 42, 104, 209, 300, and 417 psi. After each centrifuge run, the T_2 spectrum was measured again. In this context, the movable fluid saturations at various forces were calculated. It is essential to note that the maximum centrifugal force the centrifuge could apply was 417 psi. At this force, the NMR information of the movable fluids was effectively eliminated, leaving signatures of bound water. Parameters of bound water saturation as well as total movable fluid saturation were calculated using the findings from previous research (Wang et al. 2023a, b, c).

Mercury intrusion experiment

(1) High-pressure mercury intrusion

This experiment operated on the fundamental principle that mercury does not wet ordinary solids. By applying external pressure, mercury could infiltrate the pores of the material being tested. The extent of external pressure required for mercury intrusion was directly determined by the pore size; smaller pores necessitated higher pressures for infiltration. We utilized the Washburn equation to compute pore throat radius and volume by measuring different external pressures and their corresponding volumes of mercury intrusion. Mercury served as the ideal medium for this experiment due to its chemical stability, non-wetting nature, and relatively high surface tension, ensuring precise experimental results (Wang et al. 2020a, b).

(2) Constant-rate mercury intrusion

This analysis offers distinct advantages over conventional high-pressure mercury intrusion due to its quasi-static nature, maintaining constant interfacial tension and contact angle. The process involved a low constant rate of intrusion (typically 5×10^{-5} mL/min), causing variations in pore shape that affected the meniscus shape. Mercury preferentially entered larger pores, flowing through throats into connected pores, leading to pressure drops and alterations in the system's capillary pressure. The principle is based on mercury initially entering throats, with breakthroughs occurring at certain pressure levels, filling pores and causing subsequent breakthroughs (Liu et al. 2018a, b; Qiao et al. 2020a, b; Huang et al. 2021). Standard core samples were employed for these investigations (Merkel et al. 2016; Tang et al. 2017; Yang et al. 2017; Shabaninejad et al. 2018; Huang et al. 2020).

In constant-rate mercury intrusion, throats and pores were distinguished by analyzing changes in pressure. By assessing the pressure magnitudes, it became possible to calculate several key parameters.

Results

Classification and features of various diagenetic facies

Diagenetic facie are influenced by various factors, such as depositional setting, provenance, clay mineral types, and pore characteristics. The Chang 6 reservoir has experienced both constructive and destructive diagenesis. Previous studies have classified various diagenetic facies by analyzing clay and carbonate minerals. However, in this study, we proposed seven diagenetic facies based on organic matter maturity, sedimentary microfacies, diagenetic evolution characteristics, and cement and filling content. These facies are chlorite membrane cementation-intergranular pore facies (Facies I), chlorite and illite membrane cementation-intergranular pore facies (Facies II), illite cementation-intergranular pore facies (Facies III), illite and chlorite membrane cementation-dissolution facies (Facies IV), illite cementation-dissolution facies (Facies V), illite cementation facies (Facies VI), and carbonate tight cementation facies (Facies VII). Among them, Facies I to III have the best reservoir performance in a decreasing order, and they predominantly control occurrences of good reservoirs (Table 2).

The seven main diagenetic facies identified in this study are as follows:

(1) Chlorite membrane cementation-intergranular pore facies (Facies I): This diagenetic facies is prevalent in subaqueous distributary channel sands and sandy debris flow deposits. The dominant lithology consists of lithic feldspar sandstone, and the primary cement is chlorite, forming thin membranes. Intergranular pores are the main pore type, with fewer dissolution pores and other types. It represents a favorable diagenetic facies zone with well-developed reservoirs (Fig. 2a and b).
(2) Chlorite and illite membrane cementation-intergranular pore facies (Facies II): This diagenetic facies is primarily developed in subaqueous distributary chan-

Table 2 Lithology and sedimentary characteristics of reservoirs of different types of diagenetic facies

Facies type	Diagenetic facies	Clastic components (%)	Compaction strength (%)	Surface porosity (%)	Cementation rate (%)
Facies I	Chlorite membrane cementation-intergranular pore facies	Q: 33.4 F: 34.29	62.34	3.75	29.34
Facies II	Chlorite and illite membrane cementation-intergranular pore facies	Q: 25.46 F: 39.04	58.29	3.41	32.29
Facies III	Illite cementation-intergranular pore facies	Q: 27.57 F: 32.27	60.45	2.94	34.27
Facies IV	Illite and chlorite cementation and dissolution facies	Q: 27.52 F: 34.15	61.29	2.32	29.39
Facies V	Illite cementation and dissolution facies	Q: 36.9 F: 25.11	68.31	1.44	30.43
Facies VI	Illite cementation facies	Q: 35.79 F: 27.05	63.39	1.05	29.25
Facies VII	Carbonate tight cementation facies	Q: 28.38 F: 28.17	64.82	0.76	30.31

R refers to Rock Fragments, *F* stands for Feldspar, *S* indicates Sandstone, and *Q* represents Quartz. Additionally, specific minerals are denoted by Ch for Chlorite, *I* for Illite, Cal for Carbonates, *Q* for Quartz, Ka for Kaolinite, and Dol for Dolomite

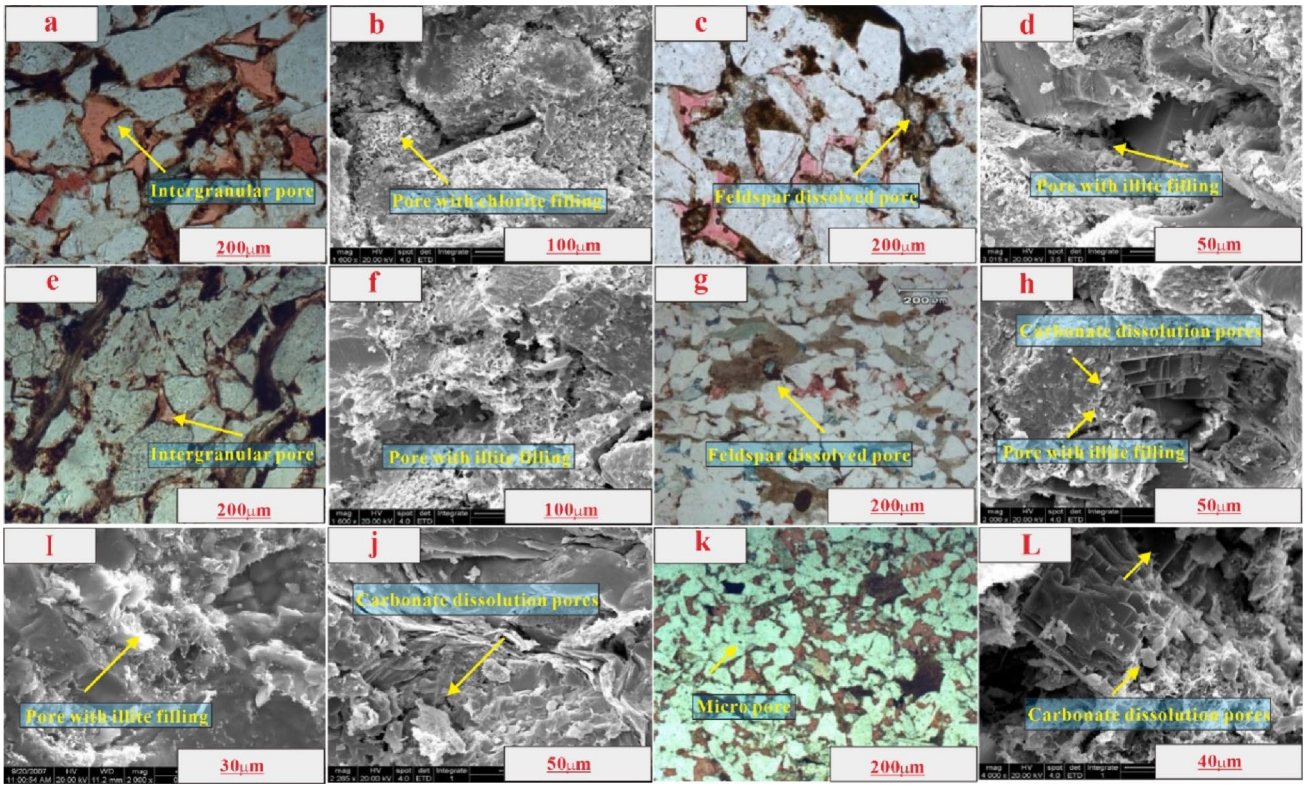

Fig. 2 SEM and thin-section images. **a–b** Thin-film-like chlorite with intergranular pores as the main pore type. **c–d** Flake-like and fibrous illite, along with thin-film-like chlorite, predominantly exhibiting intergranular pores, followed by feldspar dissolution pores. **e–f** Flake-like and fibrous illite, primarily characterized by intergranular pores. **g–h** Illite and chlorite as dominated minerals, with carbonate cementation as the secondary feature. The predominant pore type is feldspar dissolution pores. **i–j** Illite as the main mineral, with carbonate cementation as the secondary feature. Feldspar dissolution pores are the primary pore type. **k–l** Micro-pores and feldspar dissolution pores as main features, accompanied by a lesser amount of carbonate dissolution pores

nel sands and sandy debris flow deposits, with lithic feldspar sandstone as the main lithology. The cement is composed of chlorite and illite forming platy and filamentous membranes. The pore combination is mainly dissolution-intergranular pores, with dominant intergranular pores and secondary feldspar dissolution pores. It belongs to a favorable diagenetic facies zone with well-developed reservoirs (Fig. 2c and d).

(3) Illite cementation-intergranular pore facies (Facies III): This diagenetic facies is primarily developed in sandy debris flow deposits as well as some turbidite deposits. The cement consists mainly of illite, with some siderite and siliceous cement. This facies is distributed in relatively good diagenetic facies zones within the study area (Fig. 2e and f).

(4) Illite and chlorite membrane cementation-dissolution facies (Facies IV): This diagenetic facies is developed in subaqueous distributary channel sands, sandy debris flow deposits, and turbidite sand bodies. Lithic feldspar sandstone is the dominant lithology. Cement includes illite, chlorite, carbonate cement, and siliceous cement. Feldspar dissolution pores are prevalent, accompanied by some intergranular pores. This facies is relatively dominant in the diagenetic facies zones (Fig. 2g and h).

(5) Illite cementation-dissolution facies (Facies V): This diagenetic facies is well-developed in turbidite sand bodies and sandy debris flow deposits. Lithic feldspar sandstone is the main lithology. Cement consists of illite, with carbonate cement and siliceous cement present in smaller amounts. Feldspar dissolution pores are the dominant pore type, with intergranular pores also present. This facies is relatively poor in terms of reservoir properties (Fig. 2i and j).

(6) Illite cementation facies (Facies VI): This diagenetic facies is predominantly observed in turbidite sand bodies and certain sandy debris flow deposits. The lithology is characterized by lithic feldspar sandstone, with the cement mainly composed of platy illite. Feldspar dissolution pores are the dominant pore type. The reservoir properties associated with this facies are relatively poor, rendering it almost ineffective as a viable reservoir option (Figs. 2i and j).

(7) Carbonate tight cementation facies (Facies VII): This diagenetic facies is mainly developed in the channel

fringe of turbidite sand bodies. The dominant cement is carbonate cement. This facies represents a relatively poor diagenetic facies zone within the study area, with almost zero recoveries of hydrocarbons (Fig. 2k and l).

Microscopic pore structure characteristics of different diagenetic facies

Distribution of pores and throats

In Facies I, large throats predominate, followed by medium-sized ones, resulting in a relatively low displacement pressure. The capillary pressure curve tends toward the lower-left quadrant, indicating specific flow characteristics in this diagenetic facies, which represents the main flow channel in the study area (Figs. 3a and b, 4a).

In Facies II, the proportion of large pores is high, and their distribution is more uniform. Throats are mainly fine to medium-sized, and the displacement pressure is moderate. The capillary pressure curve exhibits a lower-left quadrant trend, consistent with the flow behavior observed (Figs. 3a and b, 4b).

In Facies III, the number of small pores is large, and throats are predominantly micro- to fine-sized. The capillary pressure curve shows a slight deviation toward the upper-right plateau (Figs. 3a and b, 4c).

Moving on to Facies IV, the number of small pores is large, and throats are primarily micro- to fine-sized. The capillary pressure curve exhibits a narrower plateau (Figs. 3a and b, 4d).

In Facies V, the content of large pores is high, and throats are mainly micro- to fine-sized. The capillary pressure curve tends toward the upper-right quadrant (Figs. 3a and b, 4e).

Moving to Facies VI, the content of large pores is low, and throats are primarily micro-fine-sized. The capillary pressure curve tends toward the upper-right quadrant (Figs. 3a and b, 4f).

In Facies VII, small pores and micro-fine throats predominate. When the pore-throat radius is less than 0.15 μm, the cumulative contribution of permeability exceeds 97%. This facies exhibits the highest displacement pressure, poorest reservoir properties, and the lowest mercury intrusion volume (Figs. 3a and b, 4g).

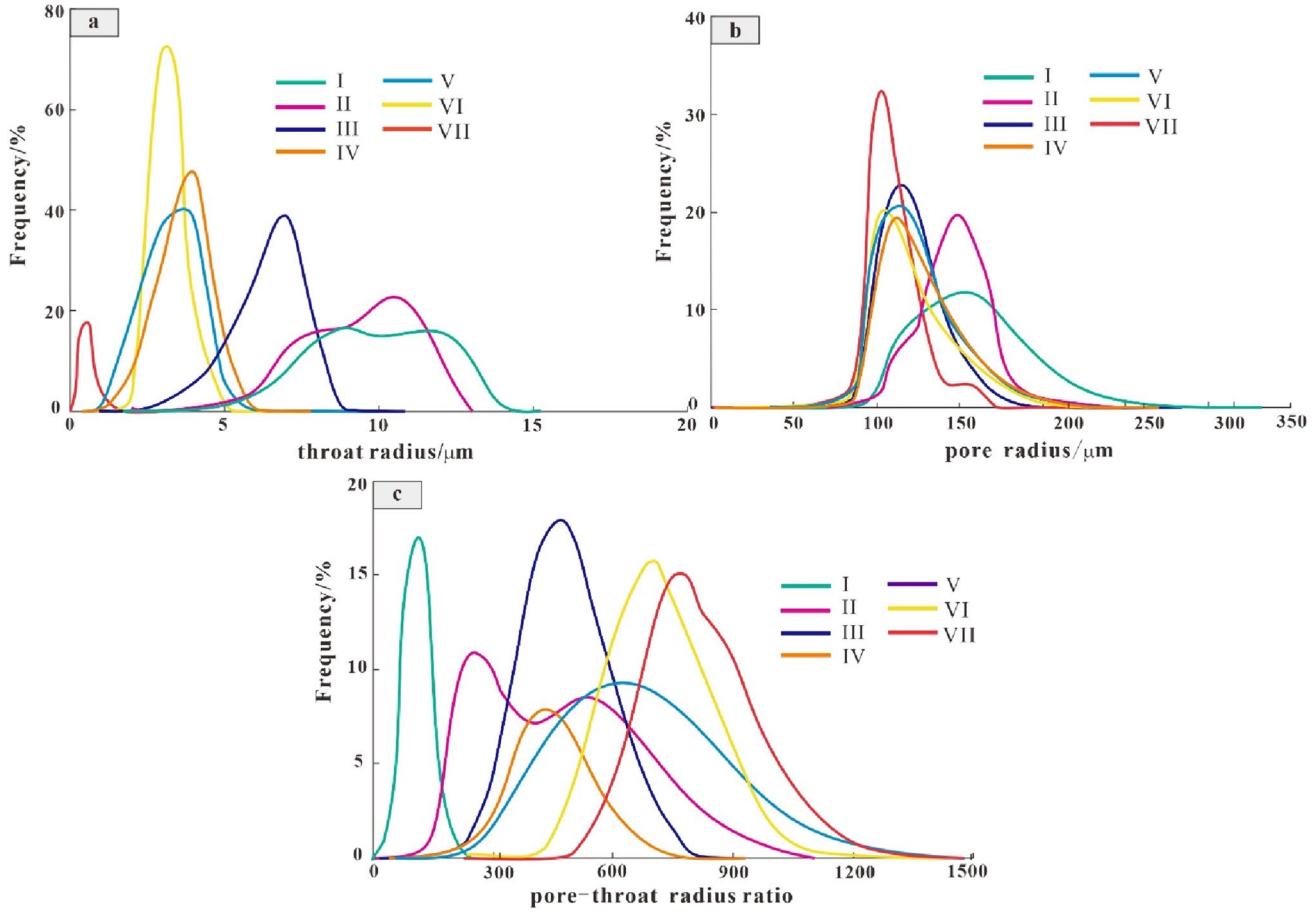

Fig. 3 Distribution of pore-throat characteristics in various diagenetic facies

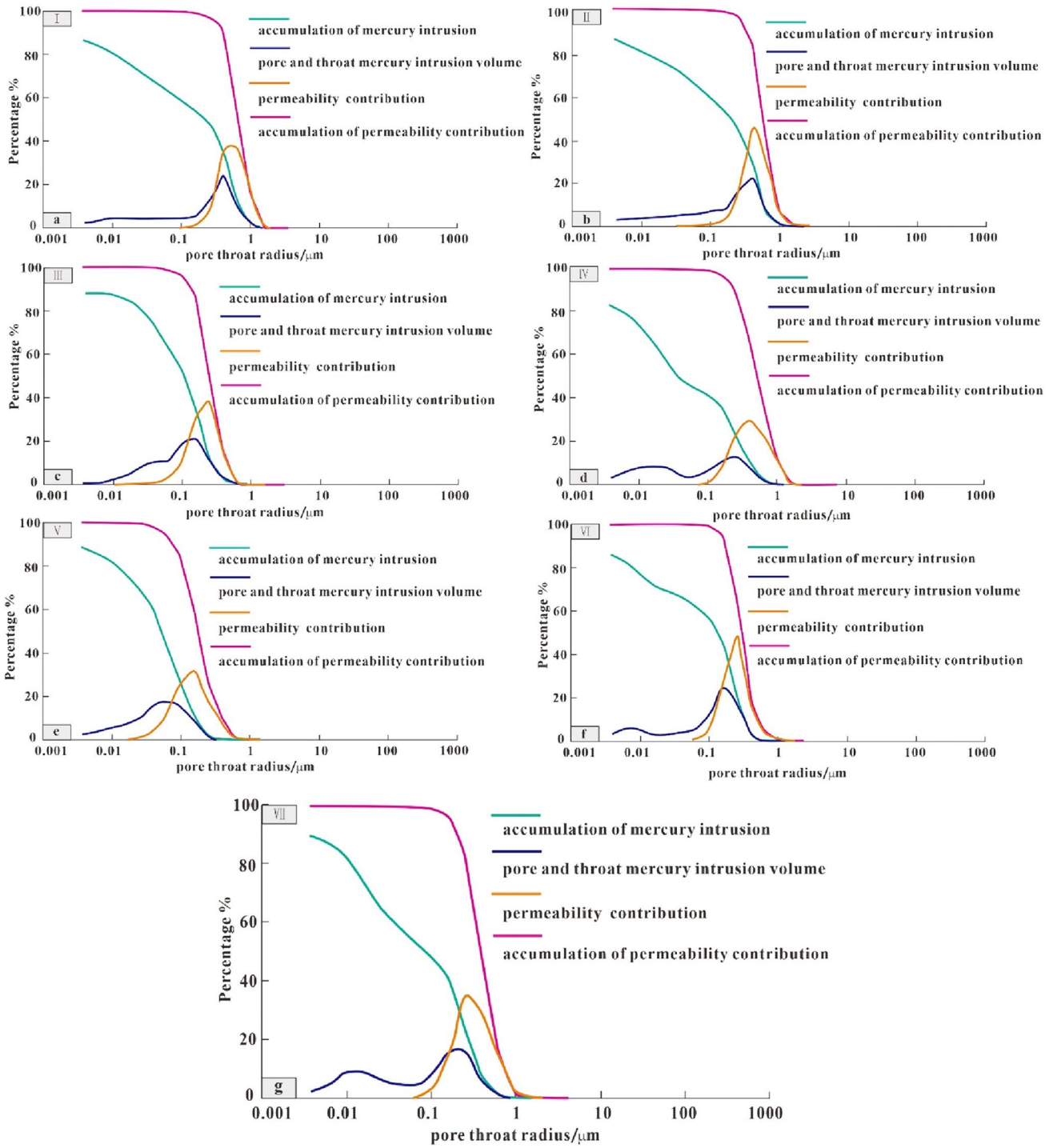

Fig. 4 Pore-throat structural characteristics in different diagenetic facies

As shown in Fig. 3a and b, Facies I exhibits the largest pore and throat radii, Facies IV to VI have similar throat radii and relatively consistent throat radius curve patterns, and Facies VII has the smallest pore and throat radii.

Distribution of pore-throat radius ratio

Figure 3c shows well-developed medium to medium-fine throats in Facies I and II. Facies I exhibits the lowest

effective pore-throat ratio with a narrow distribution range. Facies II has a relatively small pore-throat ratio, indicating a large number of small pores and large throats, resulting in weaker flow resistance and better reservoir connectivity. Facies III exhibits relatively minor differences in pore and throat sizes, with a relatively uniform distribution, lower flow resistance, and better flow capacity and pore-throat connectivity. Facies IV to VI exhibit relatively large pore-throat ratios. This indicates increasing large pores and the presence of fine and micro-fine throats. Facies VII exhibits the highest pore-throat ratio and the poorest connectivity.

Figure 4 shows a wide throat radius distribution, which suggests that the contribution to permeability is relatively dispersed. Specifically, Facies I exhibits the lowest pore-throat ratio, the largest effective throat radius, and good pore-throat sorting (Fig. 4a). It is featured by low displacement pressure, and the mercury intrusion volume curve exhibits a single peak, indicating better reservoir capacity and flow capacity. Facies III and IV have poor pore-throat sorting (Fig. 4c and d). The mercury intrusion volume curves of these two facies show a bimodal distribution, leading to decreased reservoir storage and flow capacity. The pore and throat radii of Facies III and VII are small, and the mercury intrusion volume distributions of these two facies are relatively uniform. However, the development of pore structures in these two facies is limited, resulting in low permeability contribution and poor reservoir flow capacity. In summary, Facies I exhibits the best reservoir properties, followed by Facies IV, while Facies VII has the poorest pore-throat connectivity and highest flow resistance, making it almost impossible to extract oil and gas.

Movable fluid features in various diagenetic facies based on NMR experiments

Figure 5 displays the frequency distributions of T_2 spectra for different diagenetic facies types. The T_2 spectra show both single-peak and double-peak patterns. Specifically, Facies IV to VII exhibit single peaks, while Facies I to III exhibit double peaks. The single-peak pattern with the peak located to the left of the critical value indicates small and unevenly distributed pore sizes, poor pore-throat connectivity, high heterogeneity, as well as inferior reservoir performance. In contrast, the double-peak pattern with a low-left and high-right peak suggests good connectivity between pores and throats in the first three diagenetic facies types, with larger pore sizes (Table 3 and Fig. 5).

The experimental results indicate that superior diagenetic facies types are distinguished by improved pore-throat connectivity, greater pore and throat sizes, larger saturation of movable fluids, and lower saturation of bound water. As a result, different diagenetic facies types exhibit significant variations in pore-throat characteristics, which play a crucial role in determining relative abundance of movable fluids in throats and pores (Table 1 and Fig. 5).

Discussion

Various diagenetic facies types display variations in the saturation of movable fluids. The factors influencing these differences are diverse and encompass sedimentary facies types, reservoir distribution patterns, petrophysical properties, micro-pore structure, clay mineral types, content, among others, all of which can impact movable fluid saturation. Following factors affecting movable fluid saturation in various diagenetic facies types are discussed in detail.

Reservoir properties

The correlation coefficient between movable fluid saturation and porosity is 0.3805 (Fig. 6a), while that between movable fluid saturation and permeability is stronger, at 0.6053 (Fig. 6b). A larger pore connectivity corresponds to a greater permeability, and subsequently, a larger saturation of movable fluids within the pores.

Pore and throat distributions

Pore radius and throat radius

As depicted in Fig. 7, there is a weaker correlation between movable fluid saturation and pore radius ($R^2 = 0.6398$), whereas there is a stronger correlation between movable fluid saturation and throat radius ($R^2 = 0.9415$).

Pore-throat mercury saturation

The correlation coefficient (R^2) between pore mercury saturation and movable fluid saturation across various diagenetic facies reservoirs is 0.6151 (Fig. 8a), indicating that a higher pore mercury saturation corresponds to a higher movable fluid saturation. The correlation coefficient (R^2) between throat mercury saturation and movable fluid saturation is 0.5404 (Fig. 8b). Specifically, reservoirs of Facies IV to VII exhibit fewer effective throats, smaller volumes, and smaller radii, resulting in poor connectivity and inferior reservoir properties. Consequently, most hydrocarbons accumulate in small throats and micropores, resulting in low saturation of movable fluids and reduced recovery rates. In contrast, reservoirs of Facies I to III have larger throat radii and a higher number of effective throats, indicating good connectivity and a higher content of movable fluids.

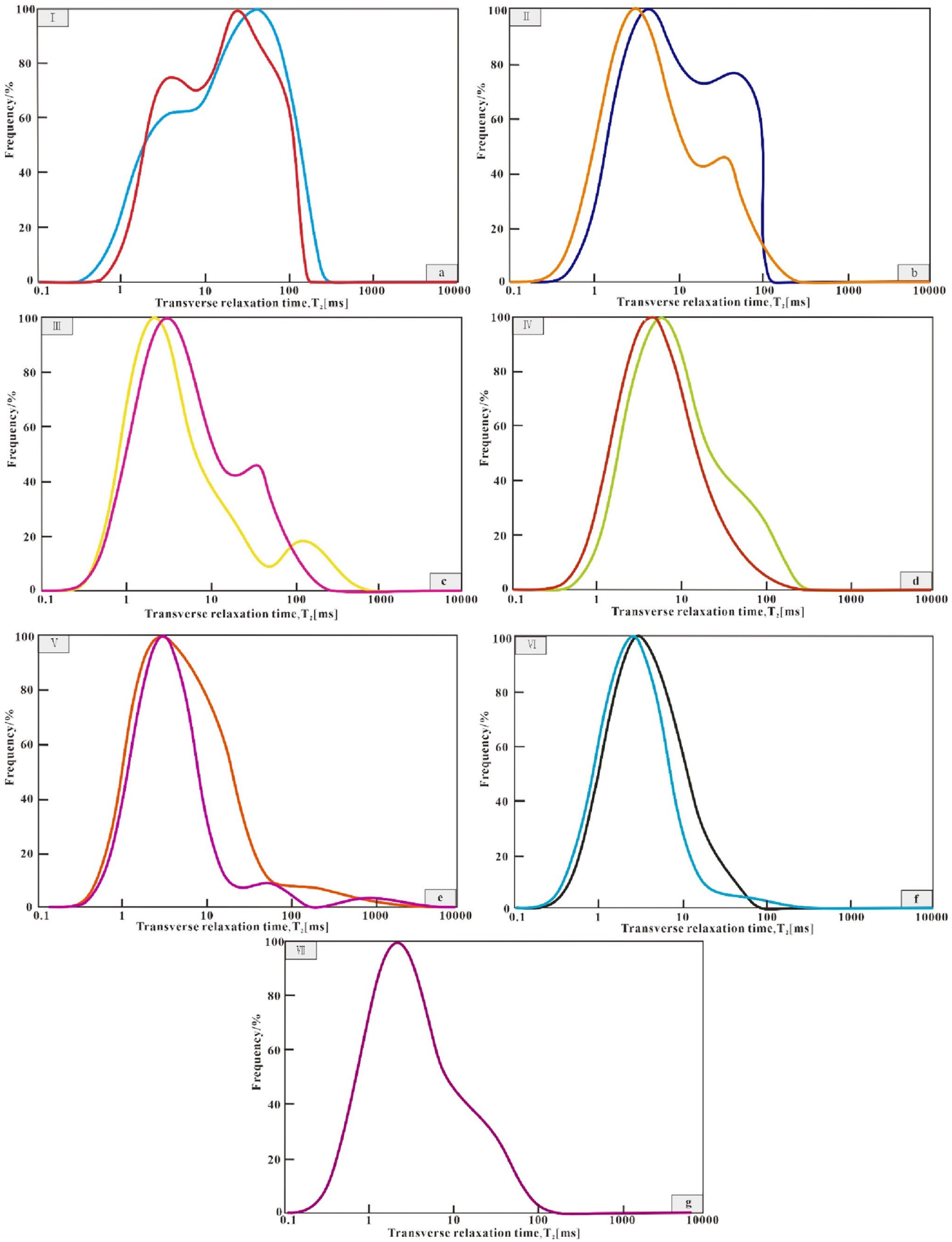

Fig. 5 NMR T_2 spectra of various types of diagenetic facies

Table 3 Various structural parameters of mercury intrusion

Classification Parameters	Facies I	Facies II	Facies III	Facies IV	Facies V	Facies VI	Facies VII
Porosity (%)	13.9	12.28	12.27	10.06	9.42	8.22	8.4
Permeability ($\times 10^{-3}\mu m^2$)	3.28	1.79	0.73	0.27	0.37	0.02	0.02
Displacement Pressure (MPa)	0.3	0.24	1.08	0.65	2.86	1.64	5.12
Median Pressure (MPa)	2.6	2.07	19.74	6.21	50.09	15.31	50.31
Maximum Pore-Throat Radius (μm)	9.7	4.93	1.59	1.34	0.71	0.37	0.15
Maximum Mercury Saturation (%)	90.72	90.7	93.81	86.83	95.53	82.96	67.31
Sorting Coefficient	2.6	2.49	2.73	2.37	2.09	1.76	1.45
Skewness Coefficient	1.9	1.58	2.05	1.76	1.83	1.53	1.37
Coefficient of variation	0.4	0.29	0.33	0.26	0.67	0.26	0.58
Mean Coefficient	10.5	10.33	11.31	10.54	9.34	9.06	10.12
Pore Type	Intergranular pore	Feldspar dissolution pore	Residual intergranular pore	Dissolution pore	Interstitial micropore	Micropore	Diagenetic fracture

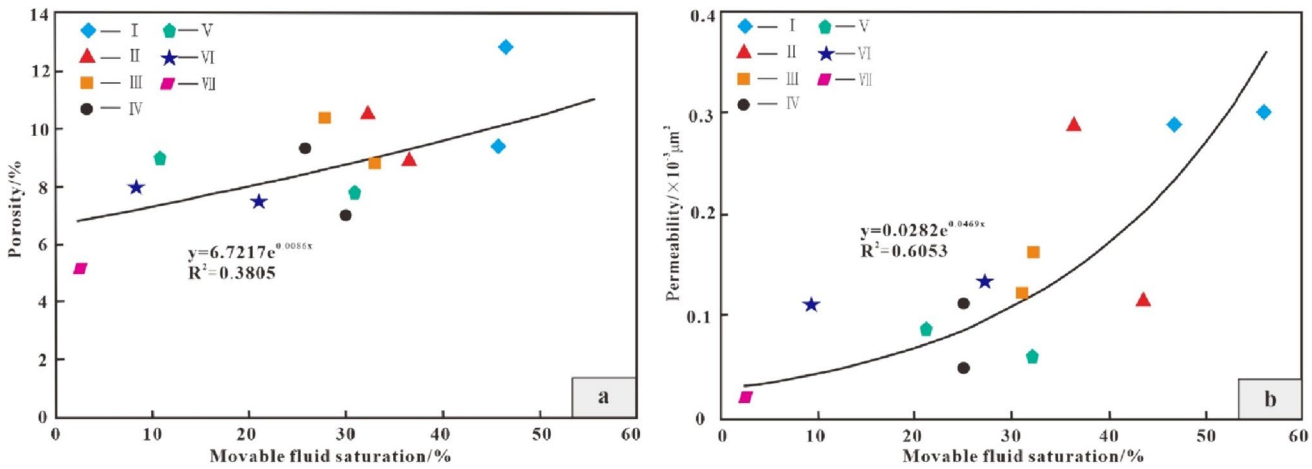

Fig. 6 Correlation between physical properties and movable fluid saturation

Pore-throat radius ratio and sorting coefficient

Figure 10a demonstrates a robust negative logarithmic relationship between the pore-throat radius ratio and the movable fluid saturation in reservoirs of various diagenetic facies, ($R^2 = 0.6104$; Fig. 9a). A larger pore-throat radius ratio is associated with a lower movable fluid saturation, and vice versa. In reservoirs of good diagenetic facies, the pore-throat radius ratio is small, indicating a uniform micro-pore-throat structure with excellent connectivity, leading to higher movable fluid saturation. Conversely, in reservoirs with poor diagenetic facies, the pore-throat radius ratio is large, signifying significant variations in pore and throat sizes and an uneven structure. Small pores surround large pores, trapping fluids in dead-end pores, resulting in limited flow and a lower movable fluid saturation.

Figure 9b shows that a larger sorting coefficient is associated with a higher movable fluid saturation ($R^2 = 0.5219$). A larger sorting coefficient indicates a better pore structure and a wider distribution range of throats, resulting in a more

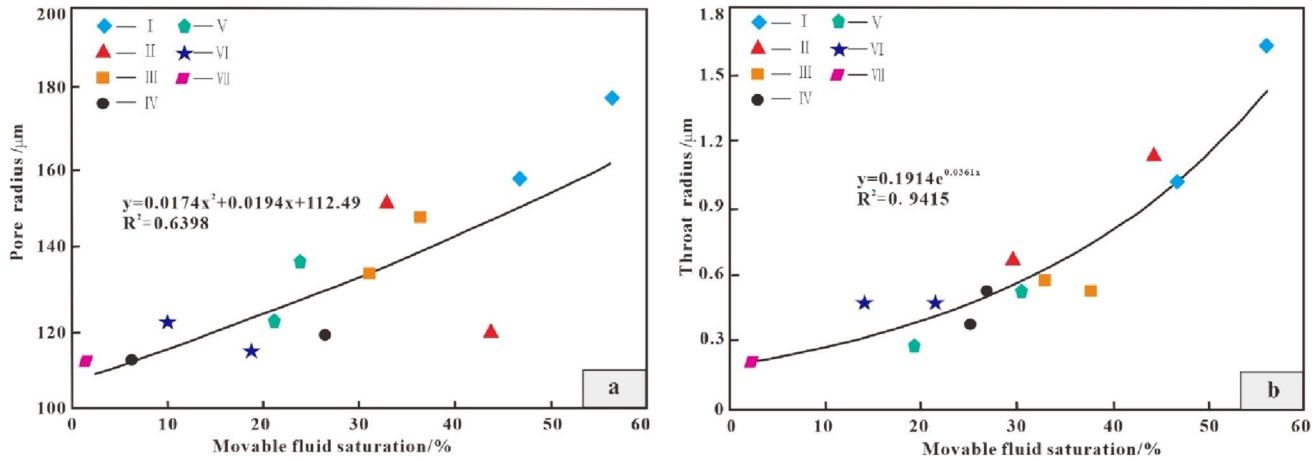

Fig. 7 Correlation between movable fluid saturation and (**a**) pore radius and (**b**) throat radius

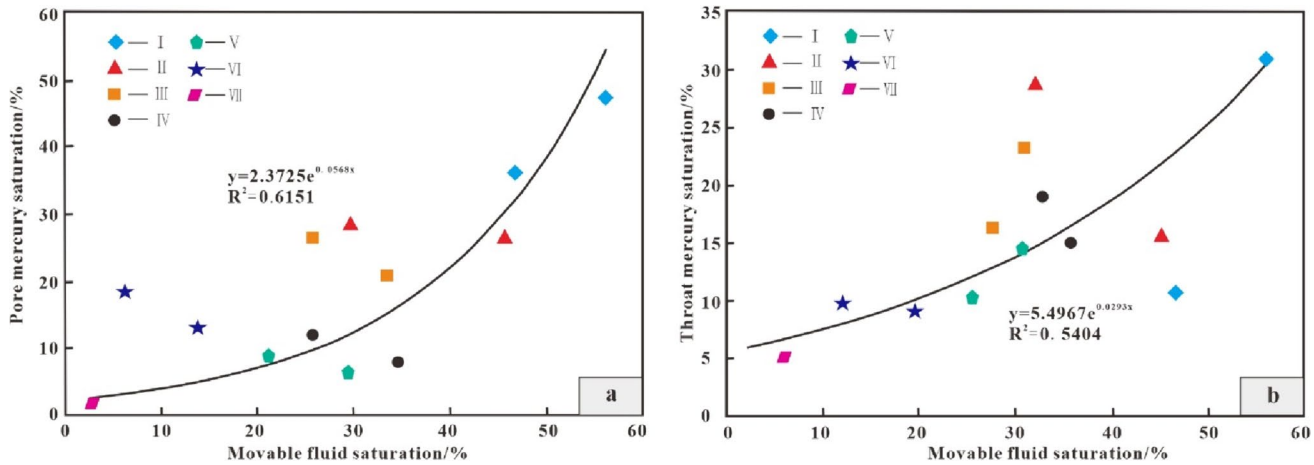

Fig. 8 Correlation between movable fluid saturation and (**a**) pore mercury saturation and (**b**) throat mercury saturation

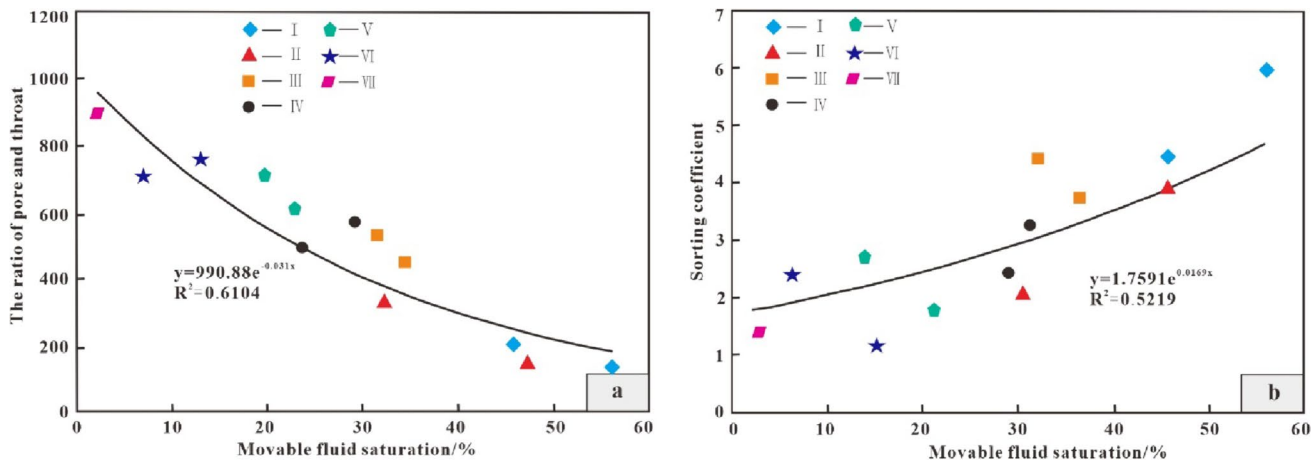

Fig. 9 Correlation between movable fluid saturation and (**a**) pore throat radius ratio and (**b**) sorting coefficient

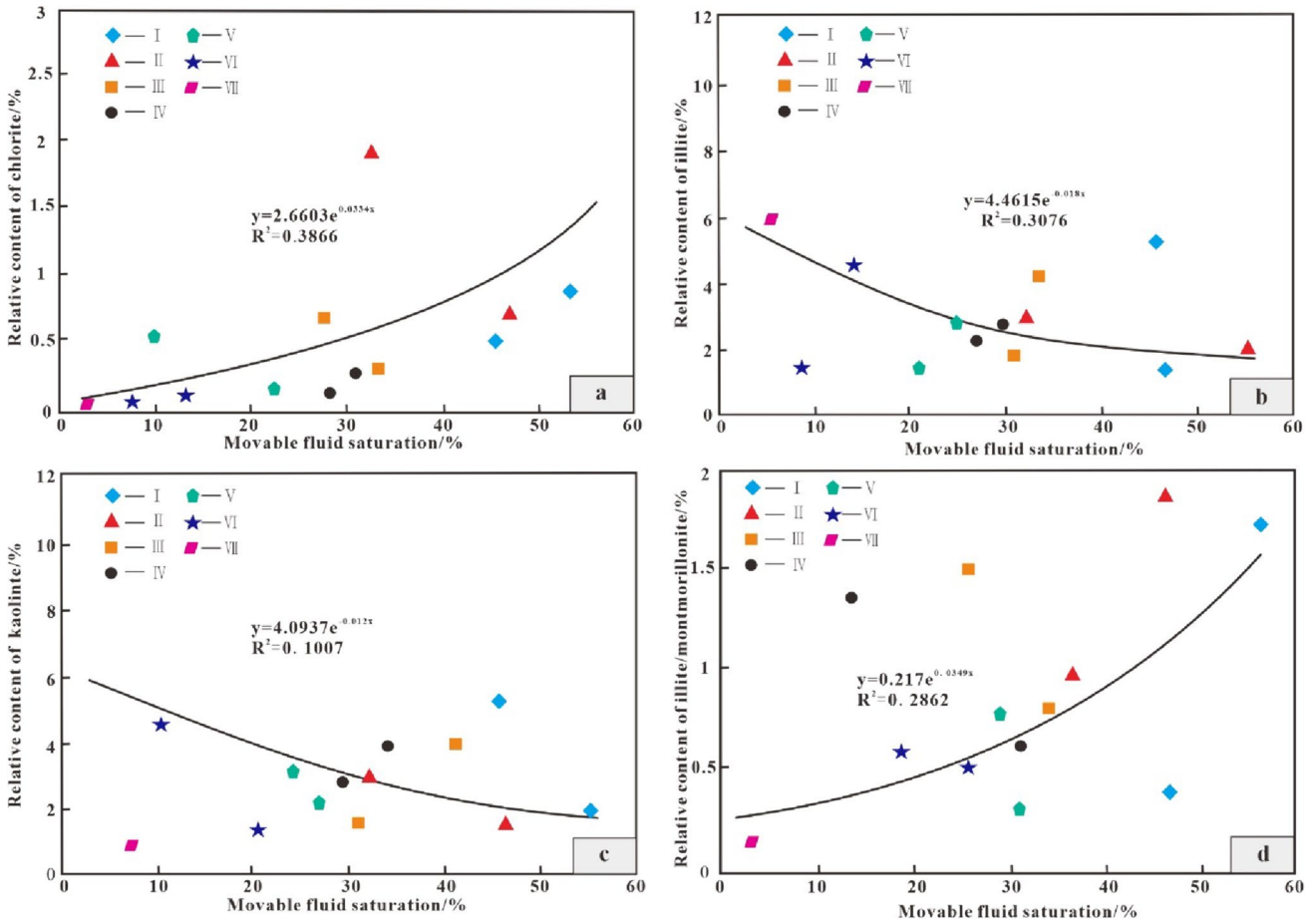

Fig. 10 Correlation between movable fluid saturation and **a** chlorite content, **b** illite content, **c** kaolinite content, **d** illite/montmorillonite content

uniform distribution of pores and throats, an increased number of large throats, enhanced flow capacity, and a higher movable fluid saturation.

In reservoirs of Facies I to III, the pore-throat radius ratio is small, and individual small pores are connected by multiple great throats, resulting in excellent permeability and smooth fluid flow. This favorable structure allows oil and gas in the pores to be easily extracted through the throats, resulting in a higher movable fluid saturation. On the other hand, in reservoirs of Facies IV to VII, the pore-throat radius ratio is large, and individual pores are connected by only a few small throats. The uneven distribution of pore and throat sizes as well as the low connectivity of pores and throats result in high heterogeneity. Consequently, fluids get trapped in the pore-throat system, making it challenging to extract, resulting in a lower recovery rate and a decreased movable fluid saturation.

Clay mineral content

Pores are filled with various clay minerals. These filling materials occupy dissolution pores and residual intergranular pores, with some adhering to the pore wall surface, resulting in significant damage to the reservoir and impacting movable fluid occurrences.

Under microscopic examination, illite exhibits filamentous and curly features. It predominantly attaches to the surface of particles and throats of connected pores, partially or completely filling the primary pores, which reduces pore connectivity. Chlorite appears as fine needle-like particles, surrounding the rock particles and lining the pores, leading to decreasing pore and throat radius, thus hindering fluid permeation. Kaolinite, with its sheet-like structure, narrows intergranular pores, increasing the content of ineffective pores, although it exerts relatively small effect on throats. The mixed layers of illite/montmorillonite display thin filamentous features and have a significant influence on movable fluid occurrence. It is evident that clay minerals of various origins present varying degrees of impact on movable fluids, with a higher degree of filling material leading to lower pore connectivity.

X-ray diffraction analysis reveals that the correlation coefficients between movable fluid saturation and llite and kaolinite contents are 0.3076 and 0.1007, respectively

(Fig. 10b and c). This indicates that the development of these clay minerals leads to reduced connectivity between pores and the presence of a significant amount of trapped fluids, thereby significantly impacting movable fluid occurrence. Movable fluid saturation shows weak positive correlations with contents of chlorite and illite/montmorillonite mixed layers ($R^2 = 0.3866$ and 0.2862, respectively; Fig. 10a and d). This suggests that these clay minerals are not very influential. Therefore, while clay mineral content does influence movable fluid occurrence, there is no significant effect from a certain clay mineral on the movable fluid occurrence.

Conclusions

1. Among the seven types of diagenetic facies, the chlorite membrane cementation-intergranular pore facies (Facies I) exhibits the largest pore and throat radii, highest exploitation potential, and the best microscopic pore structure, followed by the chlorite and illite membrane cementation-intergranular pore facies (Facies II) and illite cementation-intergranular pore facies (Facies III).
2. There is a weaker correlation between the pore-throat radius ratio and the movable fluid saturation in reservoirs of various diagenetic facies ($R^2 = 0.6104$), whereas there is a stronger correlation between movable fluid saturation and throat radius ($R^2 = 0.9415$).
3. Different diagenetic facies exhibit variations in the occurrence of movable fluids. Facies I shows uniform pore-throat radii and good connectivity, resulting in the highest movable fluid saturation and the strongest fluid mobility. Facies II and III have intermediate movable fluid saturation. Microscopic pore structure characteristics are the key factors influencing the characteristics of movable fluid saturation and causing differences in its occurrence.

Acknowledgements This work was supported by the National Natural Science Foundation of China (Grant No. 52204044), the Scientific Research Program Funded by Shaanxi Provincial Education Department (Program No. 23JY067), the Natural Science Foundation Research Project of Shanxi Province (2023-JC-QN-0389). Appreciation goes to the Changqing Oilfield Company for allowing the authors to assess the cores.

Funding This work was supported by the Scientific Research Program Funded by Shaanxi Provincial Education Department (program No. 23JY067).

Declarations

Conflict of interest The authors declare that they have no known competing financial interests or personal relationships that could have appeared to influence the work reported in this paper.

References

Al-Mahrooqi SH, Grattoni CA, Muggeridge AH, Zimmerman RW, Jing XD (2006) Pore-scale modeling of NMR relaxation for the characterization of wettability. J Pet Sci Eng 52:172–186

Chen L, Jiang Z, Liu K, Tan J, Gao F, Wang P (2017a) Pore structure characterization for organic-rich Lower Silurian shale in the Upper Yangtze Platform, South China: a possible mechanism for pore development. J Nat Gas Sci Eng 46:1–15

Chen L, Jiang Z, Liu K, Gao F (2017b) Quantitative characterization of micropore structure for organic-rich Lower Silurian shale in the Upper Yangtze Platform, South China: implications for shale gas adsorption capacity. Adv Geo-Energy Res 1(2):112–123

Cui J, Zhu R, Li S, Qi Y, Shi X, Mao Z (2019) Development patterns of source rocks in the depression lake basin and its influence on oil accumulation: Case study of the Chang 7 member of the Triassic Yanchang Formation, Ordos Basin, China. J Nat Gas Geosci 4:191–204

Dai C, Cheng R, Sun X, Liu Y, Zhou H, Wu Y, You Q, Zhang Y, Sun Y (2019) Oil migration in nanometer to micrometer sized pores of tight oil sandstone during dynamic surfactant imbibition with online NMR. Fuel 245:544–553

Daigle H, Johnson A (2016) Combining mercury intrusion and nuclear magnetic resonance measurements using percolation theory. Transp Porous Media 111:669–679

Huang H, Sun W, Ji W, Zhang R, Du K, Zhang S, Ren D, Wang Y, Chen L, Zhang X (2018) Effects of pore-throat structure on gas permeability in the tight sandstone reservoirs of the Upper Triassic Yanchang formation in the Western Ordos Basin, China. J Pet Sci Eng 162:602–616

Huang H, Li R, Jiang Z, Li J, Chen L (2020) Investigation of variation in shale gas adsorption capacity with burial depth: insights from the adsorption potential theory. J Nat Gas Sci Eng 73:103043

Huang H, Li R, Chen W, Chen L, Jiang Z, Xiong F, Guan W, Zhang S, Tian B (2021) Revisiting movable fluid space in tight fine-grained reservoirs: a case study from Shahejie shale in the Bohai Bay Basin, NE China. J Petrol Sci Eng 207:109170

Jiang M, Fang H, Liu Y, Zhang Y, Wang C (2023a) On movable fluid saturation of tight sandstone and main controlling factors—case study on the Fuyu oil layer in the Da'an oilfield in the Songliao basin. Energy 267:126476

Jiang Z, Zhu Y, Li P, Xiang J, Wang Y (2023b) Analysis of stress sensitivity and movable fluid characteristics of tight sandstone based on NMR and permeability experiments. Energy Fuels 37:16551–16563

Lai J, Wang G, Ran Y, Zhou Z, Cui Y (2016) Impact of diagenesis on the reservoir quality of tight oil sandstones: the case of Upper Triassic Yanchang Formation Chang 7 oil layers in Ordos Basin, China. J Pet Sci Eng 145:54–65

Li T, Jiang Z, Xu C, Liu B, Liu G, Wang P, Li X, Chen W, Ning C, Wang Z (2017) Effect of pore structure on shale oil accumulation in the lower third member of the Shahejie formation, Zhanhua Sag, eastern China: Evidence from gas adsorption and nuclear magnetic resonance. Mar Pet Geol 88:932–949

Li P, Sun W, Wu B, Gao Y, Du K (2018) Occurrence characteristics and influential factors of movable fluids in pores with different structures of Chang 63 reservoir, Huaqing Oilfield, Ordos Basin, China. Mar Pet Geol 97:480–492

Liu H, Yang Y, Wang F, Deng X, Liu Y, Nan J, Wang J, Zhang H (2018a) Micro pore and throat characteristics and origin of tight sandstone reservoirs: a case study of the Triassic Chang 6 and Chang 8 members in Longdong area, Ordos Basin, NW China. Pet Explor Dev 45:239–250

Liu Y, Yao Y, Liu D, Zheng S, Sun G, Chang Y (2018b) Shale pore size classification: an NMR fluid typing method. Mar Pet Geol 96:591–601

Liu X, Lai J, Fan X, Shu H, Wang G, Ma X, Liu M, Guan M, Luo Y (2020a) Insights in the pore structure, fluid mobility and oiliness in oil shales of Paleogene Funing Formation in Subei Basin, China. Mar Pet Geol 114:104228

Liu Z, Liu D, Cai Y, Yao Y, Pan Z, Zhou Y (2020b) Application of nuclear magnetic resonance (NMR) in coalbed methane and shale reservoirs: a review. Int J Coal Geol 218:103261

Mao G, Lai F, Li Z, Wei H, Zhou A (2020) Characteristics of pore structure of tight gas reservoir and its influence on fluid distribution during fracturing. J Pet Sci Eng 193:107360

Merkel A, Fink R, Littke R (2016) High pressure methane sorption characteristics of lacustrine shale from the Middle Valley Basin, Scotland. Fuel 182(1):361–372

Nie R-S, Zhou J, Chen Z, Liu J, Pan Y (2021) Pore structure characterization of tight sandstones via a novel integrated method: a case study of the Sulige gas field, Ordos Basin (Northern China). J Asian Earth Sci 213:104739

Qiao J, Zeng J, Ma Y, Jiang S, Feng S, Hu H (2020a) Effects of mineralogy on pore structure and fluid flow capacity of deeply buried sandstone reservoirs with a case study in the Junggar Basin. J Pet Sci Eng 189:106986

Qiao J, Zeng J, Jiang S, Ma Y, Feng S, Xie H, Wang Y, Hu H (2020b) Role of pore structure in the percolation and storage capacities of deeply buried sandstone reservoirs: a case study of the Junggar Basin, China. Mar Pet Geol 113:104129

Shabaninejad M, Middlelton J, Fogden A (2018) Systematic pore-scale study of low salinity recovery from Berea sandstone analyzed by micro-CT. J Pet Sci Eng 163:283–294

Tang X, Jiang Z, Jiang S, Cheng L, Zhang Y (2017) Characteristics and origin of in-situ gas desorption of the Cambrian Shuijingtuo Formation shale gas reservoir in the Sichuan Basin, China. Fuel 187:285–295

Testamanti MN, Rezaee R (2017) Determination of NMR T2 cut-off for clay bound water in shales: a case study of Carynginia Formation, Perth Basin, Western Australia. J Pet Sci Eng 149:497–503

Wang F, Zeng F (2020) Novel insights into the movable fluid distribution in tight sandstones using nuclear magnetic resonance and rate-controlled porosimetry. Nat Resour Res 29:3351–3361

Wang R, Chi Y, Zhang L, He R, Tang Z, Liu Z (2018) Comparative studies of microscopic pore throat characteristics of unconventional super-low permeability sandstone reservoirs: examples of Chang 6 and Chang 8 reservoirs of Yanchang Formation in Ordos Basin, China. J Pet Sci Eng 160:72–90

Wang Q, Chen D, Gao X, Wang F, Li J, Liao W, Wang Z, Xie G (2020a) Microscopic pore structures of tight sandstone reservoirs and their diagenetic controls: a case study of the Upper Triassic Xujiahe Formation of the Western Sichuan Depression, China. Mar Pet Geol 113:104119

Wang Q, Yang S, Glover PWJ, Lorinczi P, Qian K, Wang L (2020b) Effect of pore-throat microstructures on formation damage during miscible Co2 flooding of tight sandstone reservoirs. Energy Fuels 34:4338–4352

Wang L, Zhang Y, Zou R, Zou R, Huang L, Liu Y, Lei H (2023a) Molecular dynamics investigation of DME assisted CO2 injection to enhance shale oil recovery in inorganic nanopores. J Mol Liq 385:122389

Wang L, Zhang Y, Zou R, Zou R, Huang L, Liu Y, Meng Z, Wang Z, Lei H (2023b) A systematic review of CO2 injection for enhanced oil recovery and carbon storage in shale reservoirs. Int J Hydrogen Energy 48:37134–37165

Wang Y, Zhao X, Tang C, Zhang X, Ma C, Yi X, Tan F, Zhao D, Li J, Jing Y (2023c) Study on microscopic pore structure classification for EOR of low permeability conglomerate reservoirs in Mahu Sag. Energies 16:626

Xu S, Gou Q, Hao F, Zhang B, Shu Z, Lu Y, Wang Y (2020) Shale pore structure characteristics of the high and low productivity wells, Jiaoshiba shale gas field, Sichuan Basin, China: dominated by lithofacies or preservation condition? Mar Pet Geol 114:104211

Xu Y, Liu L, Zhu Y (2021) Characteristics of movable fluids in tight sandstone reservoir and its influencing factors: a case study of Chang 7 reservoir in the Southwestern of Ordos Basin. J Pet Explor Prod Technol 11:3493–3507

Yan J, He X, Zhang S, Feng C, Wang J, Hu Q, Cai J, Wang M (2020) Sensitive parameters of NMR T2 spectrum and their application to pore structure characterization and evaluation in logging profile: a case study from Chang 7 in the Yanchang Formation, Heshui area, Ordos Basin, NW China. Mar Pet Geol 111:230–239

Yang P, Guo H, Yang D (2013) Determination of residual oil distribution during Waterflooding in tight oil formations with NMR Relaxometry measurements. Energy Fuels 27(10):5750–5756

Yang F, Xie C, Ning Z, Krooss BM (2017) High-pressure methane sorption on dry and moisture-equilibrated shales. Energy Fuels 31:482–492

Yao Y, Liu D (2012) Comparison of low-field NMR and mercury intrusion porosimetry in characterizing pore size distributions of coals. Fuel 95:152–158

Zang Q, Liu C, Awan RS, Yang X, Lu Z, Li G, Wu Y, Feng D, Ran Y (2022) Comparison of pore size distribution, heterogeneity and occurrence characteristics of movable fluids of tight oil reservoirs formed in different sedimentary environments: a case study of the Chang 7 Member of Ordos Basin, China. Nat Resour Res 31:415–442

Zhang J, Wei C, Ju W, Qin Z, Ji Y, Quan F, Hu Y (2020) Microscopic distribution and dynamic variation of water under stress in middle and high rank coal samples. J Nat Gas Sci Eng 79:103369